NJC

PAPER

View Article Online
View Journal | View Issue

Cite this: *New J. Chem.*, 2020, **44**, 7976

NMR probe effects on *trans*-philicity and *trans*-influence ladders in square planar Pt(II) complexes†

Athanassios C. Tsipis

Received 17th March 2020,
Accepted 27th April 2020

DOI: 10.1039/d0nj01336f

rsc.li/njc

Quantitative *trans*-philicity ladders for a broad series of ligands in square planar *trans*-[Pt(PMe$_3$)$_2$(X)L]^n (n = 0, 1, 2; X = H, CO, CH$_3$, NH$_2$, OH$_2$, Cl) complexes are built employing the isotropic σ^{iso}(SO) X NMR shielding constants, calculated by DFT computational protocols at the SO-ZORA level of theory, as the *trans*-philicity descriptors. Linear relationships between the σ^{iso}(SO) X *trans*-philicity descriptors and the *R*(Pt–X) descriptors of *trans*-influence demonstrate the relation of *trans*-philicity with *trans*-influence. The electronic features of the probes are crucial factors that manipulate *trans*-philicity. The isotropic σ^{iso}(SO) X NMR descriptors of *trans*-philicity linearly correlated with the ligand electronic P_L constants and other popular electronic/structural descriptors related with the L–Pt–X bonding, revealed the origin of *trans* philicity. The *trans*-philicity ladders constructed by the six different probes go roughly parallel with only minor deviations related with the position of L in the rungs of the ladders.

Introduction

There have been numerous studies concerning the effect of a ligand on the lability of other ligands in transition metal complexes. The great majority of these investigations have been concerned with the *trans*-effect in square planar metal complexes and has been shown to be more important than the *cis*-effect which is thought to be very small and difficult to predict.[1–8] In parallel with the *trans*-effect term Pidcock *et al.*[9] introduced the *trans*-influence term. Across the periodic table the *trans*-influence operates, whereby tightly bonded ligands selectively lengthen mutually *trans* metal–ligand bonds. The *trans*-influence is fundamentally important and underpins the *trans*-effect, a kinetic rate effect where the order of substitution of ligands at a metal centre can be controlled.

Recently we aimed to gain a comprehensive understanding of the *trans*-effect/*trans*-influence phenomena for a broad series of octahedral [Cr(CO)$_5$L]$^{-/0/+}$ complexes employing the calculated σ^{iso} ^{13}C NMR shielding constants as the *trans*-effect/*trans*-influence metrics introducing the concept of *trans*-philicity to cover both kinetic and equilibrium phenomena.[10] *trans*-Philicity combines two discriminate electronic effects responsible for the electron density transfer either through the σ- or the σ- and π-subspaces. In this context the strength of *trans*-philicity could be explained in terms of σ-donation and π-back-donation, both being electronic effects. These electronic effects have previously been quantified by well-established ligand electronic parameters, such as the P_L constants defined as $P_L = E_{1/2}[\text{Cr(CO)}_6] - E_{1/2}[\text{Cr(CO)}_5\text{L}]$.[11–13]

In a following paper[14] we applied the *trans*-philicity concept in the realm of square planar Pt(II) complexes where both *trans*-influence and *trans*-effects have frequently been epitomized and probe whether and to what extent the *cis* ligands affect *trans* philicity. Having in mind that *trans*-effect/*trans*-influence phenomena operate mutually along a linear L–M–X framework we report herein on the effect of the leaving group X (used as a NMR probe) on the *trans*-philicity and *trans*-influence ladders for a broad series of square planar *trans*-[Pt(PMe$_3$)$_2$(X)L]^n (n = 0, 1, 2; X = H, CO, CH$_3$, NH$_2$, OH$_2$, Cl) complexes involving a wide variety of L (44 ligands) with diverse electronic features (σ-donor, σ-donor/π-donor, σ-donor/π-acceptor ligands). The *trans*-philicity and *trans*-influence ladders are built employing the calculated σ^{iso} X NMR shielding constants and the *R*(Pt–X) bond lengths respectively. Linear correlations between NMR parameters and the well established ligand electronic parameter P_L and other popular electronic/structural descriptors related with the L–Pt–X bonding threw light on the underlying principles and the origin of *trans* philicity and validates the broad relevance across inorganic and organometallic chemistry

---

Department of Chemistry, University of Ioannina, Ioannina 45110, Greece. E-mail: attsipis@uoi.gr

† Electronic supplementary information (ESI) available: σ^{iso}(SO) X NMR shielding constants (X = H, CH$_3$, CO, NH$_2$, OH$_2$, Cl) calculated at the SO-ZORA level of theory (Tables S1–S8); linear plots of the correlations between the σ^{iso}(SO) X NMR shielding constants (X = CH$_3$, NH$_2$, Cl) and P_L, *R*(Pt–X), WBI(Pt–X) and Q_{Pt} (Fig. S1–S4). See DOI: 10.1039/d0nj01336f

and catalysis, disposing a powerful tool in the arsenal of modelling and designing techniques.

Computational methods

All calculations were performed using the Gaussian 09, version D.01 program suite.[15] The geometries of the complexes were fully optimized, without symmetry constraints, employing the 1999 hybrid functional of Perdew, Burke, and Ernzerhof[16–19] as implemented in the Gaussian09, version D.01 program suite. The PBE0 functional mixes the Perdew–Burke–Ernzerhof (PBE) exchange energy and Hartree–Fock exchange energy in a set 3 to 1 ratio, along with the full PBE correlation energy. Geometry optimization of the square planar *trans*-$[Pt(PMe_3)_2(X)L]^n$ ($n = 0$, 1, 2; X = H, CO, CH_3, NH_2, OH_2, Cl) complexes was done in solution (benzene solvent) using the all electron SARC_ZORA basis set[20,21] for Pt central atom and the 6-31+G(d) basis set for all main group elements (E). Solvent effects were accounted for by means of the Polarizable Continuum Model (PCM) using the integral equation formalism variant (IEF-PCM) being the default self-consistent reaction field (SCRF) method.[22] Hereafter the computational protocol used in DFT calculations is abbreviated as PBE0/SARC-ZORA(Pt)∪6-31+G(d)(E)/PCM. All stationary points have been identified as minima (number of imaginary frequencies $N_{\mathrm{Imag}} = 0$). Natural Bond Orbital (NBO) population analysis was performed using Weinhold's methodology.[23,24] Magnetic shielding tensors have been computed with the gauge-including atomic orbitals DFT method,[25,26] as implemented in the Gaussian09 series of programs. The NMR shielding constants were calculated by inclusion of spin–orbit (SO) effects at the 2-component-spin–orbit-ZORA (SO-ZORA) level of theory,[27,28] using the ADF2019 code.[29] For simplicity we will denote the isotropic shielding constants as σ^{iso}(SO) calculated at the GIAO (SO-ZORA)/PBE0/TZ2P/COSMO level of theory. The GIAO (SO-ZORA)/PBE0/TZ2P/COSMO computational protocol was chosen for it was successfully used by Kaupp and co-workers[30] to probe the *trans* influence on ^1H NMR hydride shifts in square-planar platinum(II) complexes predicting accurate ^1H NMR hydride shifts matching experimental data available. We also performed calculations of the ^1H NMR hydride shifts for selected complexes employing the GIAO (SO-ZORA)/PBE0/TZ2P-J/COSMO and the results are given in the ESI,† (Table S1). It can be seen that both computational protocols provide ^1H NMR hydride shifts comparable to ^1H NMR hydride shifts calculated by Kaupp and co-workers[30] and the experiment. The deviations observed are due to the fact that in our calculations the ^1H NMR hydride shifts are calculated for the optimized geometries of the platinum(II) complexes in solution (benzene solvent), while the calculations performed by Kaupp and co-workers[30] referred to the gas-phase optimized geometries. Notice that the estimated *R*(Pt–H) bond lengths for the optimized geometries in solution, as it was expected, are longer by 0.053 Å relative to the *R*(Pt–H) bond lengths of the optimized geometries in gas-phase (Table S2, ESI†). Obviously the estimated *R*(Pt–H) bond lengths accounts well for the observed deviations of the ^1H NMR hydride shifts.

Results and discussion

Selection of the NMR probes

trans-Philicity ladders have been built for square planar *trans*-$[Pt(PMe_3)_2(X)L]^n$ ($n = 0$, 1, 2; X = H, CO, CH_3, NH_2, OH_2, Cl) complexes for a broad series of ligands L (44 ligands) employing ^1H, ^{13}C, ^{15}N, ^{17}O and ^{35}Cl NMR probes. We selected six different common NMR probes in order to answer the question whether the nature of the NMR probe affects the *trans*-philicity sequences (ladders) and the σ^{iso} *trans*-philicity descriptors. The selection of the NMR probes (X) was based on their electronic characteristics, *e.g.* employing the strong σ-donor H^- and CH_3^- ligands, the σ-donor/π-acceptor CO ligand, the σ-donor/π-donor NH_2^- and Cl^- ligands and the weak σ-donor/weak π-donor OH_2 ligand. Moreover the selected probes are ligands of broad relevance across platinum chemistry. The H^- and CH_3^- ligands are formed in catalytic processes involving activation and functionalization of C–H bonds or oxidative addition reactions.[31–34] and dehydrocoupling reactions of compounds with element-hydrogen bonds.[35] The Cl^- ligand is a good leaving group for the anticancer *cis*-$Pt(NH_3)_2Cl_2$ (*cis*-platin) drug, the OH_2 ligand occurs in the hydrolysis products of *cis*-platin, while the NH_2^- ligand models the guanine base of DNA which is generally conceived to be a major bio-molecular target of the classic Pt(II) drugs.[36–38] *trans*-Influence ladders have also been constructed employing the *R*(Pt–X) structural parameters. The relative *trans*-philicity strengths are expressed by the $\Delta\sigma^{\mathrm{iso}}$ X NMR *trans*-philicity metrics defined as the difference between the calculated σ^{iso} X NMR shielding constants for the complete set of ligands and the σ^{iso} X NMR shielding constant of the complex containing the ligand exhibiting the weakest *trans*-philicity. Similarly the relative *trans*-influence strengths are expressed by the Δ*R*(Pt–X) metrics.

trans-Philicity ladders constructed by the strong σ-donor H^- and CH_3^- NMR probes

The *trans*-philicity ladders for the *trans*-$Pt(PMe_3)_2(H)L$ and *trans*-$[Pt(PMe_3)_2(CH_3)L]^{0/+}$ complexes involving the ^1H and ^{13}C NMR probes quantified by the $\Delta\sigma^{\mathrm{iso}}$(SO) ^1H and ^{13}C NMR metrics along with the *trans*-influence ladders quantified by the Δ*R*(Pt–H) and Δ*R*(Pt–CH_3) metrics are shown in Chart 1. The calculated σ^{iso}(SO) ^1H and ^{13}C NMR shielding constants are given in the ESI† (Tables S3 and S4).

Perusal of Chart 1 reveals that the ^1H and ^{13}C NMR *trans*-philicity ladders retrieve well the experimentally established *trans* orienting series:[39]

$$H_2O \approx NO_3^- < OH^- < NH_3 < Cl^- < Br^- < I^- \approx SCN^- \approx NO_2^- \approx PR_3 \ll CO \approx C_2H_4 \approx CN^- \approx CH_3^- \approx H^-$$

Chval *et al.*[39] thoroughly investigated the mechanism of anation reactions in square planar *trans*-$Pt[(NH_3)_2T(H_2O)]^{n+}$ complexes (T = H_2O, NH_3, OH^-, F^-, Cl^-, Br^-, H_2S, CH_3S^-, SCN^-, CN^-, PH_3, CO, CH_3^-, H^-, C_2H_4) employing DFT computational methods. The authors showed that for *trans* ligands with a very strong σ-donation (*e.g.* CH_3^- and H^-) the substitution

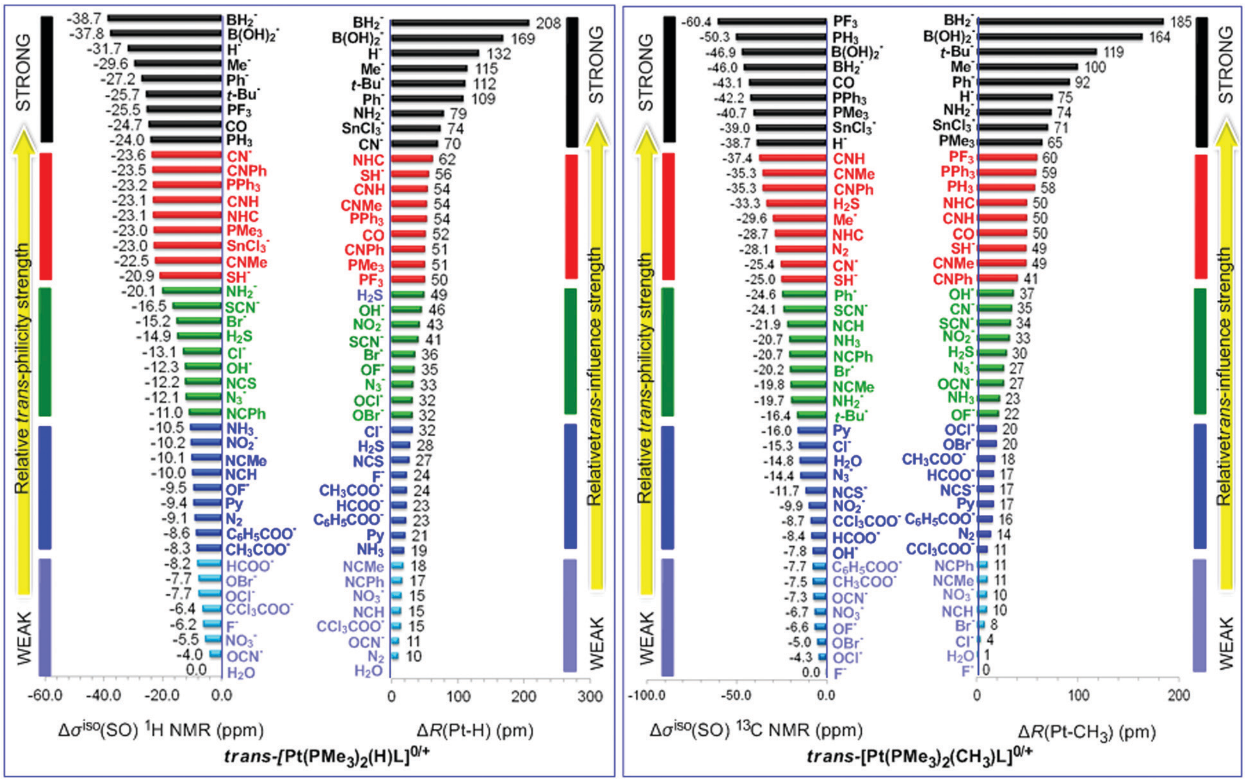

Chart 1 *trans*-Philicity ladders for the *trans*-$[Pt(PMe_3)_2(H)L]^{0/+}$ and *trans*-$[Pt(PMe_3)_2(CH_3)L]^{0/+}$ complexes quantified by the $\sigma^{iso}(SO)$ ^1H and $\sigma^{iso}(SO)$ ^{13}C NMR shielding constants referenced to the $\sigma^{iso}(SO)$ ^1H and $\sigma^{iso}(SO)$ ^{13}C shielding constants of *trans*-$[Pt(PMe_3)_2(H)(OH_2)]^+$ ($\sigma^{iso}(SO)$ ^1H = 67.0 ppm) and *trans*-$[Pt(PMe_3)_2(CH_3)(F)]$ ($\sigma^{iso}(SO)$ ^{13}C = 239.8 ppm) reference compounds respectively along with the *trans*-influence ladders quantified by the $\Delta R(Pt–H)$ and $\Delta R(Pt–CH_3)$ structural parameters referenced to $\Delta R(Pt–H)$ and $\Delta R(Pt–CH_3)$ parameters of *trans*-$[Pt(PMe_3)_2(H)(OH_2)]^+$ ($R(Pt–H)$ = 1584 pm) and *trans*-$[Pt(PMe_3)_2(CH_3)(F)]$ ($R(Pt–CH_3)$ = 2092 pm) reference compounds respectively.

proceeds by a dissociative interchange (I_d) mechanism, for *trans* ligands with strong π-back donation (*e.g.* C_2H_4) the substitution proceeds by a two step associative mechanism and for *trans* ligands with weak σ-donation and π-back-donation the substitution reactions proceed by an associative interchange (I_a) mechanism. According to the computed activation energies the T ligands follow the *trans* effect sequence:

$$C_2H_4 \gg CH_3^- \approx H^- > CO \approx CH_3S^- \approx PH_3 > CN^- \approx NO_2^-$$
$$\approx H_2S > Br^- > Cl^- > SCN^- \approx NH_3 \approx OH^- > F^- \approx H_2O$$

The calculated $\sigma^{iso}(SO)$ shielding constants for selected *trans*-$Pt(PMe_3)_2(H)L$ for which experimental data are available[40–44] (*cf.* Table S1, ESI†) demonstrate that the calculated $\sigma^{iso}(SO)$ shielding constants are accurate metrics to deploy the ligands L in reliable *trans*-philicity ladders (*trans*-philicity sequences).

Comparison of the ^1H and ^{13}C NMR *trans*-philicity ladders reveals that the two ladders are almost identical. In both ladders the strong σ-donors (H^-, Me^-, BH_2^-, $B(OH)_2^-$ and $SnCl_3^-$) occupy the rungs with very strong *trans*-philicity (black rungs), the C-donor ligands the rungs with strong *trans*-philicity (red rungs) while the N- and O-donor ligands occupy the rungs with moderate to weak *trans*-philicity (green and blue rungs). However in many cases the ligands L follow different orders along the *trans* orienting series. In particular the strong σ-donors *t*-Bu^- and Ph^- ligands occupy remarkably different rungs in the ^1H and ^{13}C NMR *trans*-philicity ladders. The *t*-Bu^- and Ph^- ligands are found in the black rungs of the ^1H NMR *trans*-philicity ladder and the green rungs of the ^{13}C NMR *trans*-philicity. However this is not the case in the respective *trans*-influence sequences (ladders). It is important to be noticed that Kaupp and co-workers[30] applying quantitative relativistic DFT methodology in a series of square planar Pt(II) complexes and exploring correlations between the calculated ^1H shifts and the *trans* ligand influence series established the *trans*-influence sequence: $NO_3^- < ONO^- < NO_2^- < Cl^- < Br^- < SCN^- \approx I^- < CN^- < Ph^- < Me^- < SiR_3^- \approx BR_2^-$, which is exactly the same with the *trans*-philicity series shown in the $\sigma^{iso}(SO)$ ^1H NMR *trans*-philicity ladder (Chart 1). In a following publication Kaupp and co-workers[45] presented the results of a extensive investigation of the ligand effects on the NMR shifts of metal-bound nuclei in 5d transition-metal complexes, encompassing both $5d^8$ and $5d^{10}$ electron configurations, with related effects even for $5d^6$ complexes using relativistic quantum-chemical analyses. The authors showed that the *trans* ligand effects on the shieldings are exclusively dominated by two mixed σ-/π-type spinors.

Generally with only minor deviations related with the position of a few ligands in the *trans*-influence and ^1H NMR *trans*-philicity ladders the two ladders go parallel to each other.

Phosphanes, nitriles, CO, NO_2^-, OH^-, and N_2 exert strong *trans*-influence (R(Pt–H) = 1625–1638 pm), while the O-donor ligands along with halides, isocyanides, SH_2, N_3^-, NCS^-, Py, NH_3, N_2 and OH_2 ligands exert moderate to weak *trans*-influence (R(Pt–H) = 1584–1620 pm). Noteworthy in both ^1H and ^{13}C NMR *trans*-philicity ladders the *trans*-philicity of phosphane ligands follows the order: $PF_3 > PH_3 > PPh_3 > PMe_3$. According to the σ-donor/π-acceptor ratio, PF_3, PH_3 and PMe_3 follow the trend[46] $PF_3 < PH_3 < PMe_3$, while according to the $\nu(C{\equiv}O)$ stretching vibrational frequencies for $Ni(CO)_3L$ complexes follow the order[47] $PF_3 > PPh_3 > PMe_3$ in line with the *trans*-philicity sequence for the phosphane ligands. Similarly the ^1H and ^{13}C NMR *trans*-philicity ladders reproduce the experimentally established *trans*-influence sequences, $Br^- > Cl^- > F^-$ and $NH_3 >$ Py.

In the *trans*-$[Pt(PMe_3)_2(CH_3)L]^{0/+}$ complexes the *trans*-influence ladder match better to the ^{13}C NMR *trans*-philicity ladder. The two ladders are almost similar showing only minor local order inversions of a few ligands along the *trans* orienting series. In both ladders the strong σ-donor (H^-, Me^- and *t*-Bu^-, $SnCl_3^-$), the C-donor (CO and isocyanides) along with the BH_2^-, $B(OH)_2^-$ and phosphane ligands occupy the rungs with strong to very strong *trans*-influence and *trans*-philicity. Similarly the N- and O-donor ligands occupy the rungs with moderate to weak *trans*-influence and *trans*-philicity, but in many cases follow different orders along the *trans* orienting series.

trans-Philicity ladder constructed by the σ-donor/π-acceptor CO probe

The *trans*-philicity ladder for the *trans*-$[Pt(PMe_3)_2(CO)L]^{+/2+}$ complexes quantified by the $\Delta\sigma^{iso}$ ^{13}C NMR metrics along with the *trans*-influence ladder quantified by the ΔR(Pt–CO) metrics are shown in Chart 2. The calculated σ^{iso}(SO) ^{13}C NMR shielding constants are given in the ESI† (Table S5).

The ^{13}CO NMR *trans*-philicity ladder matches better to the ^1H NMR than the $^{13}CH_3$ NMR ladders (Chart 1). Comparison of the aforementioned *trans*-philicity ladders illustrates clearly that the electronic features of the probes are crucial factors that tune deploy of ligands L in the *trans*-philicity ladders. In particular nitriles NCR (R = H, Me, Ph) occupy the pale blue rungs with weak *trans*-philicity in the ^{13}CO NMR *trans*-philicity ladder and the blue rungs with moderate *trans*-philicity in the $^{13}CH_3$ and ^1H NMR *trans*-philicity ladders. It can also be seen that various classes of ligands in the three ladders follow the trends:

Strong σ-donor ligands:

^1H ladder: $SnCl_3^- <$ *t*-$Bu^- < Ph^- < Me^- < H^- < BH_2^- < B(OH)_2^-$

$^{13}CH_3$ ladder: *t*-$Bu^- < Ph^- < Me^- < SnCl_3^- < H^- < B(OH)_2^- < BH_2^-$

^{13}CO ladder: $SnCl_3^- < Ph^- < Me^- < H^- <$ *t*-$Bu^- < B(OH)_2^- < BH_2^-$

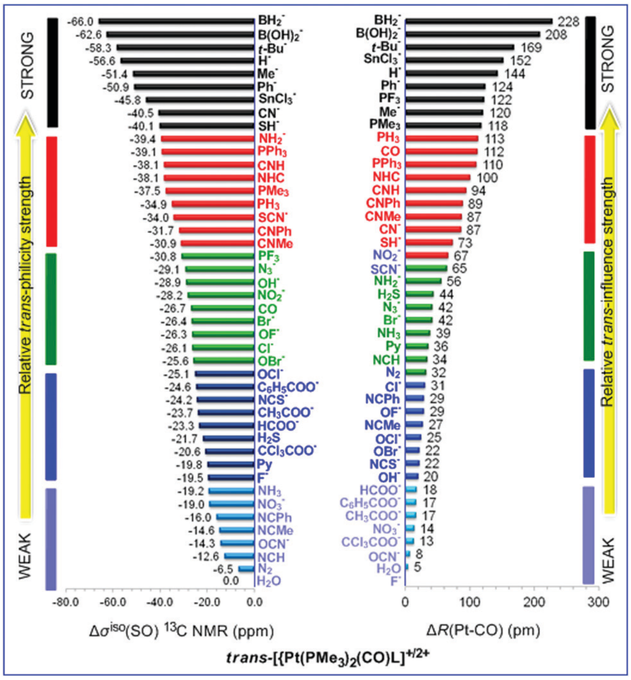

Chart 2 *trans*-Philicity ladder for the *trans*-$[Pt(PMe_3)_2(CO)L]^{+/2+}$ complexes quantified by the σ^{iso}(SO) ^{13}C NMR shielding constants referenced to the σ^{iso}(SO) ^{13}C shielding constants of *trans*-$[Pt(PMe_3)_2(CO)(OH_2)]^{2+}$ (σ^{iso}(SO) ^{13}C = 48.8 ppm) reference compound along with the *trans*-influence ladder quantified by the ΔR(Pt–CO) structural parameters referenced to ΔR(Pt–CO) parameters of *trans*-$[Pt(PMe_3)_2(CO)(F)]^+$ (R(Pt–CO) = 1936 pm) reference compound.

C-Donor ligands:

^1H ladder: $CNMe < NHC < CNH < CNPh < CN^- < CO$

$^{13}CH_3$ ladder: $CN^- < NHC < CNPh < CNMe < CNH < CO$

^{13}CO ladder: $CO < CNMe < CNPh < NHC < CNH < CN^-$

N-Donor ligands:

^1H ladder: $N_2 < py < NCH < NCMe < NO_2^- < NH_3 < NCPh < N_3^- < NCS^- < NH_2^-$

$^{13}CH_3$ ladder: $NO_2^- < NCS^- < N_3^- < py \ll NH_2^- < NCMe < NCPh < NH_3 < NCH < N_2$

^{13}CO ladder: $N_2 < NCH < NCMe < NCPh < NH_3 < py < NCS^- < NO_2^- < N_3^- < NH_2^-$

O-Donor ligands:

^1H ladder: $OH_2 < OCN^- < NO_3^- < CCl_3COO^- < OCl^- < OBr^- < HCOO^- < CH_3COO^- < C_6H_5COO^- < OF^- < OH^-$

$^{13}CH_3$ ladder: $OCl^- < OBr^- < OF^- < NO_3^- < OCN^- < CH_3COO^- < C_6H_5COO^- < OH^- < HCOO^- < CCl_3COO^- < OH_2$

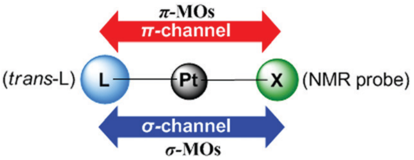

Scheme 1 Electron density transfer pathways (σ- and π-channels) between the *trans* L ligands and the X NMR probes supported by σ- and π-MOs.

^{13}CO ladder: $OH_2 < OCN^- < NO_3^- < CCl_3COO^- < HCOO^- < CH_3COO^- < C_6H_5COO^- < OCl^- < OBr^- < OF^- < OH^-$

Phosphanes:

^{1}H ladder: $PMe_3 < PPh_3 < PH_3 < PF_3$

^{13}CO ladder: $PMe_3 < PPh_3 < PH_3 < PF_3$

^{13}CH$_3$ ladder: $PF_3 < PH_3 < PMe_3 < PPh_3$

The deviations observed might be due to the synergic contribution of the σ-donor and π-acceptor capacity of the probes to the mutual electron density transfer L → Pt → CO pathways (channels) taken place through the σ- and/or the σ- and π-subspaces (Scheme 1).

According to Scheme 1 the electronic features of the *trans* L ligands and X NMR probes are the crucial determinants of the net charge transfer from the *trans* L ligands to X NMR probes that manipulates *trans*-philicity. In this context *trans*-philicity (*trans* effect/*trans*-influence) originates from electronic effects. The electronic nature of *trans*-philicity accounts well for the positions of the σ-donor/π-donor SH$^-$, SCN$^-$and NH$_2^-$ ligands in rungs of higher *trans*-philicity relative to their positions in the ^{1}H and ^{13}CH$_3$ NMR ladders. Coordination of the σ-donor/π-donor ligands to [Pt(PMe$_3$)$_2$(CO)]$^{2+}$ reference standard adds more electron density on the CO probe by electron density transfer through the π-channel that increases the downfield shifts, hence increasing *trans*-philicity and moving the positions of σ-donor/π-donor ligands in rungs of higher *trans*-philicity in the ^{13}CO NMR *trans*-philicity ladder.

Generally in the *trans*-influence ladder the majority of the ligands occupy the proper rungs of the ladder, *e.g.* the strong σ-donors and phosphanes occupy the rungs of very strong *trans*-influence, the C-donors the rungs of strong *trans*-influence, the N-donors, hypohalites, SH$_2$ and Cl$^-$ the rungs of moderate *trans*-influence and the O-donors along with F$^-$ the rungs of weak *trans*-influence.

trans-Philicity ladder constructed by the strong σ-donor/π-donor NH$_2$ probe

The *trans*-philicity ladder for the *trans*-[Pt(PMe$_3$)$_2$(NH$_2$)L]$^{0/+}$ complexes quantified by the $\Delta\sigma^{iso}$ ^{15}N NMR metrics along with the *trans*-influence ladder quantified by the ΔR(Pt–NH$_2$) parameters are shown in Chart 3. The calculated σ^{iso}(SO) ^{15}N NMR shielding constants are given in the ESI† (Table S6).

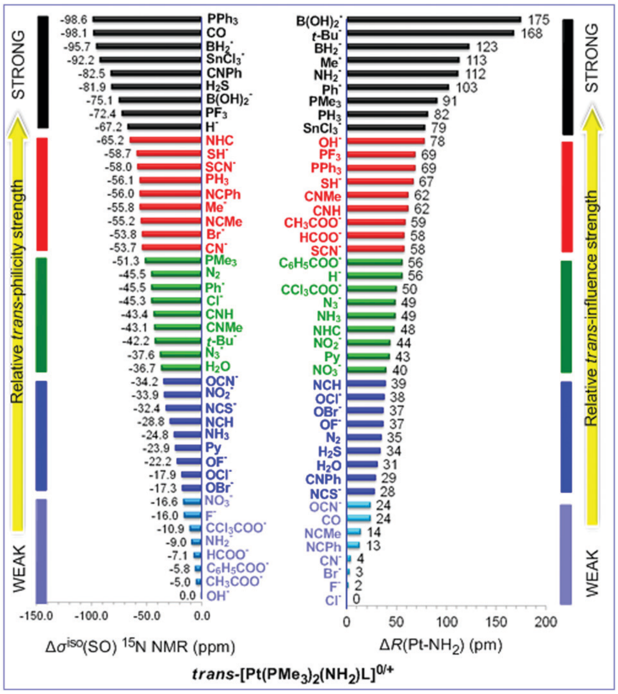

Chart 3 *trans*-Philicity ladder for the *trans*-[Pt(PMe$_3$)$_2$(NH$_2$)L]$^{0/+}$ complexes quantified by the σ^{iso}(SO) ^{15}N NMR shielding constants referenced to the σ^{iso}(SO) ^{15}N shielding constants of *trans*-[Pt(PMe$_3$)$_2$(NH$_2$)(OH)] (σ^{iso}(SO) ^{15}N = 322.5 ppm) reference compound along with the *trans*-influence ladder quantified by the ΔR(Pt–NH$_2$) structural parameters referenced to ΔR(Pt–NH$_2$) parameters of *trans*-[Pt(PMe$_3$)$_2$(NH$_2$)(Cl)] (R(Pt–NH$_2$) = 2042 pm) reference compound.

In the ^{15}N NMR *trans*-philicity ladder the O-donor ligands occupy the rungs with weak *trans*-philicity, the strong σ-donor and phosphane ligands the rungs with strong *trans*-philicity, while the N- and C-donor ligands occupy rungs with strong, moderate and weak *trans*-philicity. Noteworthy the ^{15}N NMR *trans*-philicity ladder matches better to the ^{13}CH$_3$ ladder, with only minor deviations related with the position of L in the rungs of the two ladders, rather than to the ^{13}CO and ^{1}H NMR *trans*-philicity ladders. However in the *trans*-influence ladder remarkable changes in the *trans*-influence sequences relative to the ^{15}N NMR *trans*-philicity sequences are observed. Specifically in the *trans*-influence ladder the O-donor ligands are placed in the rungs of moderate to strong *trans*-influence. In the *trans*-influence sequences phosphanes are placed in the rungs with weak to very weak *trans*-influence. The same holds true for some of the C-donor ligands (CO, CN- and isocyanides) and N-donor ligands (NHC, Py, NH$_3$ and nitriles) deviating from the experimentally established *trans* orienting series.

trans-Philicity ladder constructed by the weak σ-donor/weak π-donor OH$_2$ probe

The *trans*-philicity ladder for the *trans*-[Pt(PMe$_3$)$_2$(OH$_2$)L]$^{+/2+}$ complexes quantified by the $\Delta\sigma^{iso}$ ^{17}O NMR descriptors along with the *trans*-influence ladder quantified by the ΔR(Pt–OH$_2$) structural parameters are shown in Chart 4. The calculated

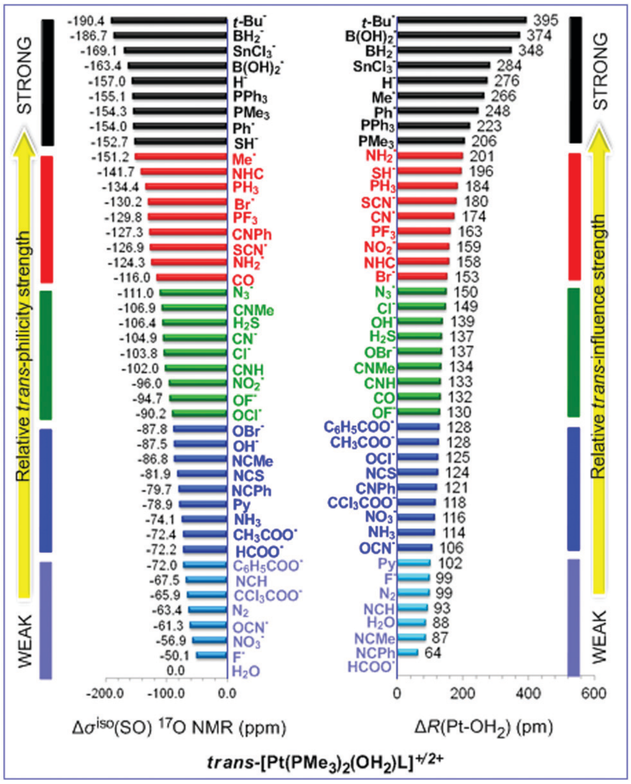

Chart 4 *trans*-Philicity ladder for the *trans*-[Pt(PMe$_3$)$_2$(OH$_2$)L]$^{+/2+}$ complexes quantified by the σ^{iso}(SO) ^{17}O NMR shielding constants referenced to the σ^{iso}(SO) ^{17}O shielding constants of [*trans*-Pt(PMe$_3$)$_2$(OH$_2$)(OH$_2$)]$^{2+}$ (σ^{iso}(SO) ^{17}O = 513.8 ppm) reference compound along with the *trans*-influence ladder quantified by the ΔR(Pt–OH$_2$) structural parameters referenced to ΔR(Pt–OH$_2$) parameters of [*trans*-Pt(PMe$_3$)$_2$(OH$_2$)(OOCH)]$^+$ (R(Pt–OH$_2$) = 2100 pm) reference compound.

σ^{iso}(SO) ^{17}O NMR shielding constants are given in the ESI† (Table S7).

Interestingly the ^{17}O NMR *trans*-philicity ladder is almost identical with the ^{1}H NMR (Chart 1) and ^{13}CO NMR (Chart 2) *trans*-philicity ladders with only marginal deviations related with local inversion of the *trans*-philicity order of some ligands. On the other hand the *trans*-influence ladder quantified by the R(Pt–OH$_2$) parameters deploy *trans*-influence sequences, which do not match the experimentally established *trans* orienting series. In effect the strong σ donor BH$_2^-$, B(OH)$_2^-$, H$^-$, SnCl$_3^-$, Me$^-$, *t*-Bu$^-$ and Ph$^-$ anionic ligands along with phosphanes, CN$^-$, NH$_2^-$, SH$^-$, SCN$^-$ and NO$_2^-$ ligands occupy the rungs with very strong *trans*-influence in the *trans*-influence ladder in line with the experimentally established *trans* orienting series. However the O-donor (RCOO$^-$, OX$^-$, OCN$^-$ and OH$^-$) ligands along with NHC, N$_3^-$, Br$^-$, Cl$^-$, NCS$^-$ and PH$_3$ occupy the rungs with strong to moderate *trans*-influence deviating from the experimentally established *trans* orienting series. Similarly the C-donor (isocyanides and CO) ligands along with the N-donor (nitriles, NH$_3$, Py and N$_2$) and PF$_3$ ligands are placed in the rungs of weak *trans*-influence also deviating from the experimentally established *trans* orienting series.

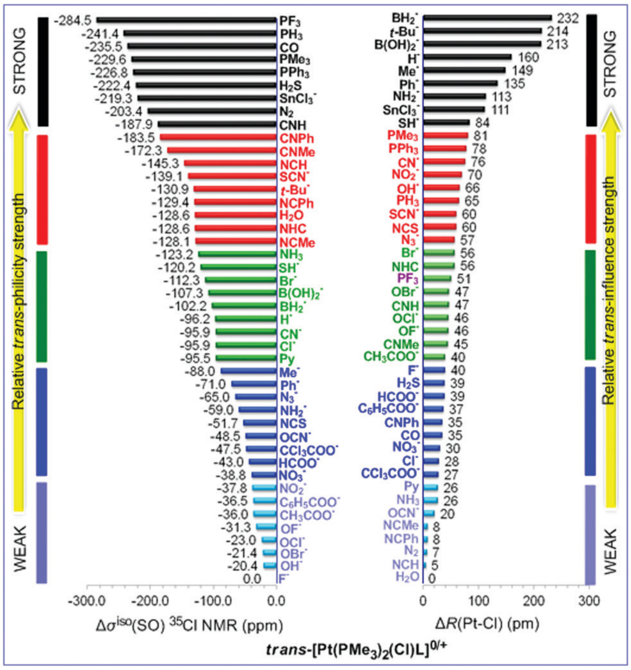

Chart 5 *trans*-Philicity ladder for the *trans*-[Pt(PMe$_3$)$_2$(Cl)L]$^{0/+}$ complexes quantified by the σ^{iso}(SO) ^{35}Cl NMR shielding constants referenced to the σ^{iso}(SO) ^{35}Cl shielding constants of *trans*-[Pt(PMe$_3$)$_2$(Cl)(F)] (σ^{iso}(SO) ^{35}Cl = 1225.2 ppm) reference compound along with the *trans*-influence ladder quantified by the ΔR(Pt–Cl) structural parameters referenced to ΔR(Pt–Cl) parameters of *trans*-[Pt(PMe$_3$)$_2$(Cl)(OH$_2$)]$^+$ (R(Pt–Cl)) = 2355 pm) reference compound.

trans-Philicity ladder constructed by the moderate σ-donor/weak π-donor Cl probe

Chart 5 shows the *trans*-philicity ladder for the *trans*-[Pt(PMe$_3$)$_2$(Cl)L]$^{0/+}$ complexes quantified by the $\Delta\sigma^{iso}$(SO) ^{35}Cl NMR descriptors along with the *trans*-influence ladder quantified by the ΔR(Pt–Cl) structural descriptors. The calculated σ^{iso}(SO) ^{35}Cl NMR shielding constants are given in the ESI† (Table S8).

The ^{35}Cl NMR *trans*-philicity ladder has an analogous structure to the corresponding ^{1}H, ^{13}CO and ^{17}O NMR *trans*-philicity ladders with only minor deviations related with the positions of a few ligands in the rungs of the ladders. Surprisingly the rungs with very strong *trans*-philicity are occupied by the C-donor (isocyanides and CO) ligands, instead of the strong σ-donor, phosphane and SH$_2$ ligands. The strong σ-donor ligands are moved to the regions of strong and moderate *trans*-philicity. In the regions of strong and moderate *trans*-philicity are also found the N-donor (nitriles, Py, NH$_3$, NH$_2^-$, N$_3^-$ and NO$_2^-$) along with the SH$^-$, SCN$^-$, CN$^-$, Br$^-$, Cl$^-$ and OH$_2$ ligands, while the O-donor (RCOO$^-$, OX$^-$, OCN$^-$ and OH$^-$) ligands and F$^-$ are correctly placed in the rungs of weak *trans*-philicity.

In the *trans*-influence ladder the strong σ donor BH$_2^-$, B(OH)$_2^-$, H$^-$, SnCl$_3^-$, Me$^-$, *t*-Bu$^-$ and Ph$^-$ anionic ligands along with NH$_2^-$, OH$^-$, SH$^-$, CN$^-$, Br$^-$, N$_3^-$ and SCN$^-$ ligands are placed in the rungs of very strong and strong *trans*-influence, in line with the experimentally established *trans* orienting series. The O-donor (RCOO$^-$, OX$^-$, OCN$^-$) ligands along with NO_2^-, F^-, Cl^- and NCS^- occupy the rungs with strong to moderate *trans*-influence. The C-donor (isocyanides and CO) along with the N-donor (nitriles, NH_3, Py and N_2) ligands occupy the rungs of weak *trans*-influence deviating from the experimentally established *trans* orienting series.

Correlations between the isotropic σ^{iso}(SO) X NMR shielding constants and the ligand electronic parameter P_L

In order to scrutinize the underlying principles and the origin of *trans* philicity and threw some light on the still intriguing physics of the *trans*-influence phenomena we investigated relationships between the isotropic σ^{iso}(SO) X (X = ^1H, $^{13}CH_3$, ^{13}CO, ^{15}N, ^{17}O and ^{35}Cl) shielding constants and the well established ligand electronic parameters P_L (a measure of the overall electron attracting or releasing quality of L).[14] Representative linear plots of the σ^{iso}(SO) X (X = ^1H, ^{13}CO, $^{17}OH_2$) *vs.* P_L are shown in Fig. 1. Linear plots of the σ^{iso}(SO) X (X = $^{13}CH_3$, $^{15}NH_2$, ^{35}Cl) *vs.* P_L correlations are given in the ESI† (Fig. S1).

Inspection of Fig. 1 and Fig. S1 (ESI†) reveals that accurate linear relationships are obtained for similar subsets of ligands L. In the σ^{iso}(SO) ^1H *vs.* P_L, σ^{iso}(SO) ^{17}O *vs.* P_L (Fig. 1) and σ^{iso}(SO) $^{15}NH_2$ *vs.* P_L (Fig. S1, ESI†) the ligands are grouped into four families, in the σ^{iso}(SO) ^{13}CO *vs.* P_L, and σ^{iso}(SO) ^{35}Cl *vs.* P_L correlations (Fig. S1, ESI†) into two ligand families, while in the σ^{iso}(SO) $^{13}CH_3$ *vs.* P_L, correlations into three ligand families.

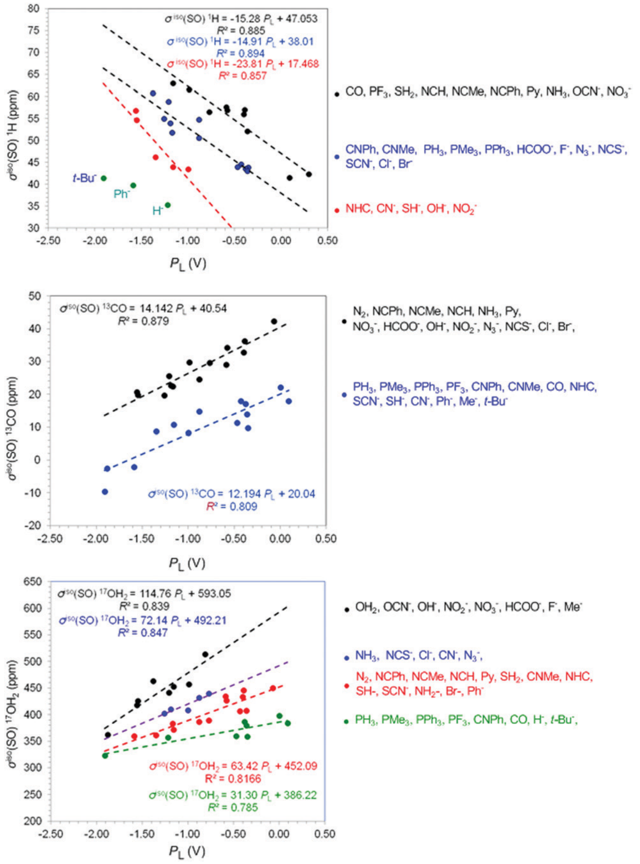

Fig. 1 Linear plots of the σ^{iso}(SO) X (X = ^1H, ^{13}CO and $^{17}OH_2$) shieldings *vs.* P_L correlations for square planar *trans*-$[Pt(PMe_3)_2(X)L]^n$ (n = 0, 1, 2; X = H, CO, OH_2) complexes calculated by the GIAO(SO-ZORA)/PBE0/TZ2P/COSMO computational protocol in benzene solution.

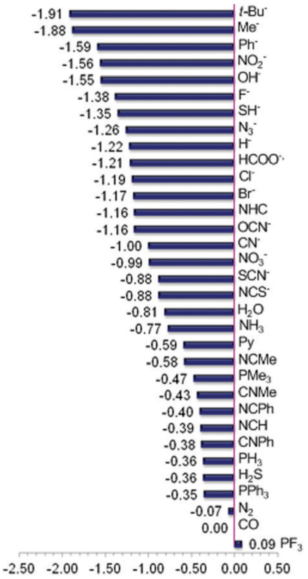

Chart 6 P_L constants ladder (values taken from ref. 14).

Generally the O-, N-, C- and σ-donor ligands form their own families and in some cases are mixed with phosphane and S-donor ligands. Notice that the three and two ligand families result from the mixing of O- and N-donor ligands in the same family. Noteworthy in the σ^{iso}(SO) ^1H *vs.* P_L correlations (Fig. 1) and the σ^{iso}(SO) X (X = $^{13}CH_3$, $^{15}NH_2$ and ^{35}Cl) *vs.* P_L correlations (Fig. S1, ESI†) increase of the negative value of P_L constant (increase of the electron releasing capacity of L) increases the downfield shifts of the σ^{iso}(SO) X NMR shielding constants. Conversely in the σ^{iso}(SO) X (X = ^{13}CO and $^{17}OH_2$) *vs.* P_L correlations (Fig. 1) increase of the negative value of P_L constant increases the upfield shifts of the σ^{iso}(SO) X NMR shielding constants. It should be noticed that the values of the P_L constants, taken from ref. 14 are presented herein in from of a P_L constants ladder (Chart 6).

The different NMR probe effects on the σ^{iso}(SO) X (X = ^{13}CO and $^{17}OH_2$) and σ^{iso}(SO) X (X = ^1H, $^{13}CH_3$, $^{15}NH_2$ and ^{35}Cl) could be explained by the synergism of the *trans* L and X ligands to balance the electron density transfer along the L–Pt–X framework through the σ- and π-subspaces that affects the X NMR shielding constants (compare the overall electron attracting or releasing quality of the X NMR probe given in Chart 6). The H^- and CH_3^- NMR probes are strong σ-donors ligands. The same holds true for the NH_2^- and Cl^- NMR probes with their σ-donor capacity enhanced by the weak π-donor capacity of these probes (these ligands are found at the top of the P_L ladder). On the other hand H_2O and CO NMR probes are weak σ-donors with the σ-donor capacity of the latter further diminished by its strong π-acceptor capacity (H_2O and CO ligands are found at the low part of the P_L ladder).

Correlations between the σ^{iso}(SO) X NMR descriptors of *trans*-philicity and the *R*(Pt–X) descriptors of *trans*-influence

To demonstrate weather *trans*-philicity is related with the *trans*-influence phenomenon we investigated relationships between

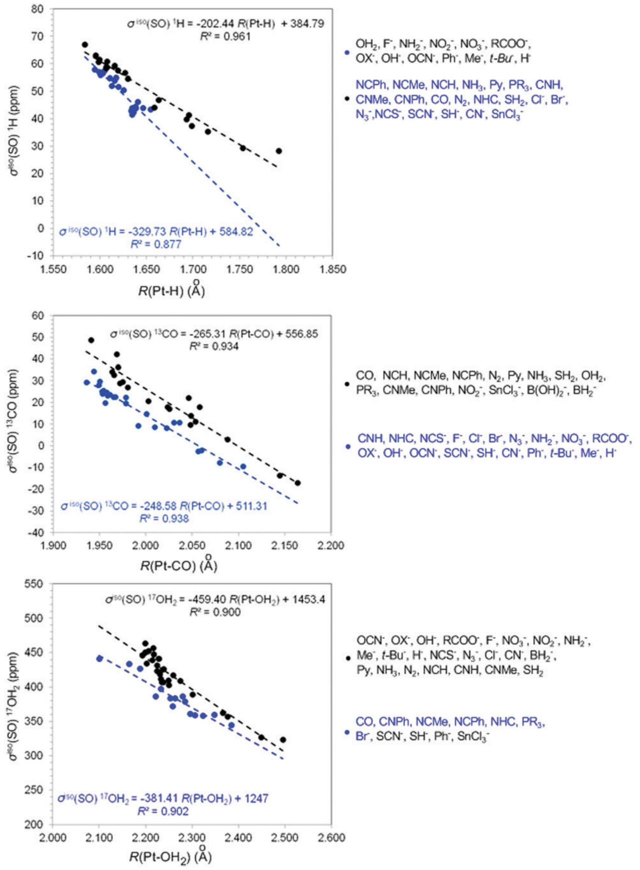

Fig. 2 Linear plots of the σ^{iso}(SO) X (X = ^{1}H, ^{13}CO and ^{17}OH$_2$) shieldings *vs.* *R*(Pt–X) correlations for square planar *trans*-[Pt(PMe$_3$)$_2$(X)L]^n (n = 0, 1, 2; X = H, CO, OH$_2$) complexes calculated by the GIAO(SO-ZORA)/PBE0/TZ2P/COSMO computational protocol in benzene solution.

the σ^{iso}(SO) X (X = ^{1}H, ^{13}CH$_3$, ^{13}CO, ^{15}N, ^{17}O and ^{35}Cl) *trans*-philicity descriptors and the *R*(Pt–X) descriptors of *trans*-influence. The linear plots of the σ^{iso}(SO) X (X = ^{1}H, ^{13}CO, ^{17}OH$_2$, ^{13}CH$_3$, NH$_2$ and ^{35}Cl) *vs.* *R*(Pt–X). Correlations are shown in Fig. 2 and Fig. S2 (ESI†).

Accurate correlation equations can be drawn from two ligand families for the σ^{iso}(SO) X (X = ^{1}H, ^{13}CO, ^{17}OH$_2$) *vs.* *R*(Pt–X) correlation, three ligand families for the σ^{iso}(SO) X *vs.* *R*(Pt–X) X = CH$_3$ and NH$_2$ correlation and four ligand families for the σ^{iso}(SO) ^{35}Cl *vs.* *R*(Pt–Cl) correlations. The first family in the σ^{iso}(SO) X *vs.* *R*(Pt–X) X = H, CO, OH$_2$ correlations involves most of the O-donor ligands mixed with some of the strong σ-donor and N-donor ligands, while the second ligand family involves all the remaining ligands.

In the σ^{iso}(SO) ^{13}CH$_3$ *vs.* *R*(Pt–CH$_3$) and σ^{iso}(SO) ^{15}NH$_2$ *vs.* *R*(Pt–NH$_2$) correlations the first family involves strong σ-donor BH$_2^-$, B(OH)$_2^-$ and Ph$^-$ ligands mixed with OH$^-$, OX$^-$, OCN$^-$, NO$_2^-$, NH$_2^-$ and F$^-$ ligands. In the second family one finds N-donor ligands along with CN$^-$, SCN$^-$, SH$^-$ and SnCl$_3^-$ ligands, while the third family involves the C-donor, nitriles, phosphanes, halides, H$_2$S and H$_2$O ligands.

The linear relationships for the σ^{iso}(SO) X (X = ^{1}H, ^{13}CO, ^{17}OH$_2$, ^{13}CH$_3$, NH$_2$ and ^{35}Cl) *vs.* *R*(Pt–X) correlations show that the increase of the *R*(Pt–X) descriptor of *trans*-influence increases the upfield shifts of the σ^{iso}(SO) X descriptors of *trans*-philicity.

Correlations between the σ^{iso}(SO) X NMR shielding constants and the WBI(Pt–X) and Q_{Pt} electronic parameters

To probe further the electronic nature of *trans* philicity we investigated possible relationships of the σ^{iso}(SO) X (X = ^{1}H, ^{13}CH$_3$, ^{13}CO, ^{15}NH$_2$, ^{17}OH$_2$ and ^{35}Cl) shielding constants and natural bond orbital (NBO) parameters, namely the Wiberg Bond Index of the Pt–X bond, WBI(Pt–X) and the natural atomic charge on Pt metal center Q_{Pt}. Representative linear plots of the σ^{iso}(SO) X *vs.* WBI(Pt–X) and σ^{iso}(SO) X *vs.* Q_{Pt} (X = H, CO, OH$_2$) correlations are shown in Fig. 3 and 4 respectively. The linear plots of the σ^{iso}(SO) X *vs.* WBI(Pt–X) and σ^{iso}(SO) X *vs.* Q_{Pt} (X = CH$_3$, NH$_2$, Cl) correlations are given in the ESI† (Fig. S3 and S4).

Inspection of the linear plots given in Fig. 3 and Fig. S3 (ESI†) reveals that accurate linear equations can be drawn from distinct ligand families. For the σ^{iso}(SO) X *vs.* WBI(Pt–X) (X = H, CO, OH$_2$, CH$_3$) correlations accurate linear equations are obtained for three ligand families, while for the σ^{iso} (SO) X *vs.* WBI(Pt–X) (X = NH$_2$, Cl) correlations from four ligand families. These ligand families are given in Fig. 3 and Fig. S3 (ESI†). It can also be seen that in all linear relationships the increase of WBI(Pt–X) (increase of the covalency of the Pt–X bond)

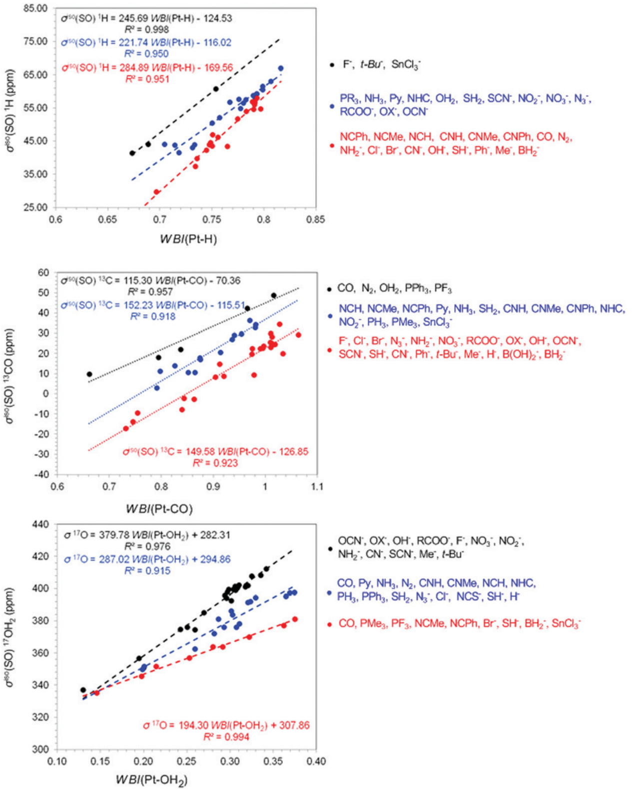

Fig. 3 Linear plots of the σ^{iso}(SO) X (X = ^{1}H, ^{13}CO and ^{17}OH$_2$) shieldings *vs.* WBI(Pt–X) correlations for square planar *trans*-[Pt(PMe$_3$)$_2$(X)L]^n (n = 0, 1, 2; X = H, CO, OH$_2$) complexes calculated by the GIAO(SO-ZORA)/PBE0/TZ2P/COSMO computational protocol in benzene solution.

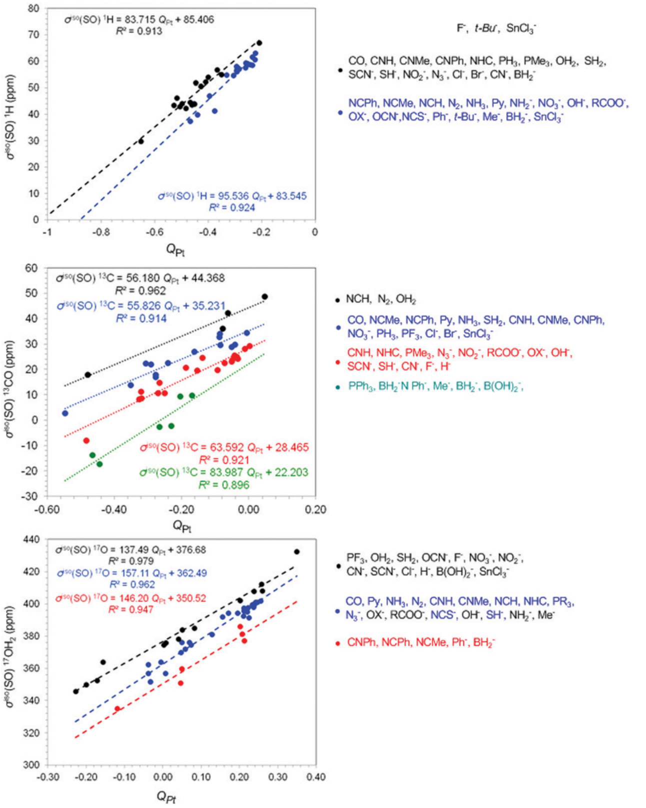

Fig. 4 Linear plots of the σ^{iso}(SO) X (X = ^{1}H, ^{13}CO and ^{17}OH$_2$) shieldings *vs.* Q_{Pt} correlations for square planar *trans*-[Pt(PMe$_3$)$_2$(X)L]^n (n = 0, 1, 2; X = H, CO, OH$_2$) complexes calculated by the GIAO(SO-ZORA)/PBE0/TZ2P/COSMO computational protocol in benzene solution.

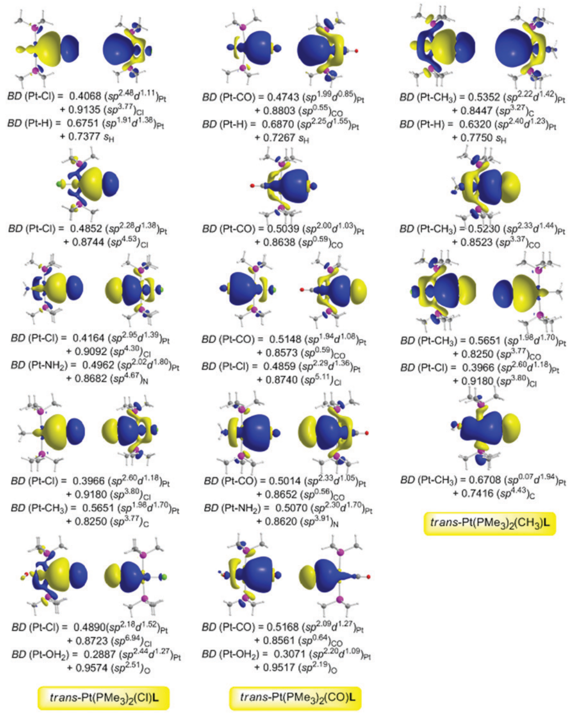

Scheme 2 3D plots and composition of the bonding natural orbitals localized on the Pt–X and L–Pt bonds for selected *trans*-[Pt(PMe$_3$)$_2$(X)L]^n (n = 0, 1, 2; X = H, CO, OH$_2$) complexes. The X and L ligands are selected on the basis of their electronic characteristics (σ-donor, σ-donor/π-acceptor, σ-donor/π-donor).

increases the downfield shift of σ^{iso}(SO) X shielding constants. In this context the relation of the *trans*-philicity and *trans*-influence with the covalency of Pt–X bond demonstrates clearly the electronic origin of the two phenomena. Scheme 2 shows the 3D plots and composition of the natural bonding orbitals BD (Pt–X) and BD(L–Pt) for selected *trans*-Pt(PMe$_3$)$_2$(X)L (X = Cl, CO, CH$_3$) complexes.

Taking into consideration that the primary determinant of *trans*-philicity is likely to be covalent contributions to bonding, whether they arise from σ donation or π back-donation, in the formation of the L → Pt dative bond electron density is transferred towards the coordination site *trans* to L. Interestingly, the σ^{iso}(SO) X shieldings linearly correlate with the calculated WBI(Pt–X) parameters, a measure of the covalency of Pt–X bond, demonstrating that the covalent bonding contributions to the Pt–X bond and the net charge transfer from the ligand L to Pt metal center are the key factors that manipulate *trans*-philicity. The bonding σ(Pt–X) NBOs are constructed from the interaction of the sp^{m}d^n hybrid orbitals of the Pt(II) metal center with the s or sp^k hybrid orbitals of X and are described as $\sigma(\text{Pt–X}) = c_1(\text{sp}^m\text{d}^n)_{\text{Pt}} + c_2(\text{sp}^k)_{\text{X}}$. The covalency of the σ(Pt–X) NBOs increases (higher WBI(Pt–X) values) by increasing the overlap of the $(\text{sp}^m\text{d}^n)_{\text{Pt}}$ and $(\text{sp}^k)_{\text{X}}$ hybrid orbitals. Accordingly increase of the overlap results from the overlap of more diffuse $(\text{sp}^m\text{d}^n)_{\text{Pt}}$ hybrid orbitals that exhibit higher d-orbital character illustrating the crucial role of 5d orbitals of Pt(II) in modulating the propagation of spin–orbit effects on the σ^{iso}(SO) shielding constants.

The *trans*-philicity descriptors are linearly correlated with the natural atomic charges on the Pt central atom, Q_{Pt}, (Fig. 4 and Fig. S5, ESI†). For the σ^{iso}(SO) X *vs.* Q_{Pt} correlations accurate linear equations are obtained from two, three or four ligand families, which are given in Fig. 4 and Fig. S4 (ESI†). At this point it is important to be noticed that in all correlations studied the grouping of the ligands into families is almost similar. The linear plots of the σ^{iso}(SO) X *vs.* Q_{Pt} correlations show that the increase of electron density on the Pt central atom, Q_{Pt} induces upfield shifts of σ^{iso}(SO) X shielding constants.

Conclusions

Quantitative *trans*-philicity ladders for a broad series of ligands (44 ligands) in square planar *trans*-[Pt(PMe$_3$)$_2$(X)L]^n (n = 0, 1, 2; X = H, CO, CH$_3$, NH$_2$, OH$_2$, Cl) complexes are built by the isotropic σ^{iso}(SO) X NMR *trans*-philicity descriptors. We also deployed the ligands under study in *trans*-influence sequences employing the R(Pt–X) structural descriptors. Accordingly the relation of *trans*-philicity with *trans*-influence validates the *trans*-philicity concept, as a unified term, avoiding confusion in the ambiguous use of the kinetic *trans*-effect and the structural *trans*-influence terms, often encountered in coordination chemistry. The relative *trans*-philicity strengths are expressed by the $\Delta\sigma^{iso}$(SO) X NMR *trans*-philicity metrics defined as the difference between the calculated σ^{iso}(SO) X NMR shielding constants for the complete set of ligands and the σ^{iso}(SO) X NMR shielding constant of the complex containing the ligand exerting the weakest *trans*-philicity phenomenon. Similarly the relative *trans*-influence strengths are expressed by the ΔR(Pt–X) structural metrics. Important results are summarized as follows.

The NMR *trans*-philicity ladders built for square planar *trans*-$[Pt(PMe_3)_2(X)L]^n$ (n = 0, 1, 2; X = H, CO, CH_3, NH_2, OH_2, Cl) complexes, involving a broad series of ligands (44 ligands) with diverse electronic features go roughly parallel to *trans*-influence ladders built by the ΔR(Pt–X) descriptors.

The NMR *trans* philicity descriptors depend on the nature of the NMR probe. The electronic effects of the NMR probes (σ-donor, σ-donor/π-acceptor, σ-donor/π-donor) tune the electron density transfer L → Pt → X pathways, thus affecting the σ^{iso} X *trans*-philicity descriptors. For the σ-donor NMR probes (^1H, $^{13}CH_3$ and $^{17}OH_2$) the electron density transfer L → Pt → X takes place only through the σ-subspace (σ-channel), whereas for the σ-donor/π-acceptor ^{13}CO and σ-donor/π-donor $^{15}NH_2$ and ^{35}Cl NMR probes the electron density transfer takes place through both the σ- and π-subspaces (σ- and π-channels). The synergic contribution of the σ- and π-electronic effects of L and X to balance the electron density transfer along the L → Pt → X framework are the crucial factors that manipulate *trans*-philicity. Generally very strong σ-donor ligands and σ-donor/π-acceptor ligands exert strong *trans*-philicity, σ-donor/π-donor ligands exert moderate *trans*-philicity, while weak σ-donors exert the weakest *trans*-philicity.

Excellent linear relationships between the isotropic σ^{iso}(SO) X shielding constants and the well established ligand electronic parameter P_L and other popular electronic/structural descriptors related with the L–Pt–X bonding threw light on the underlying principles and the electronic origin of *trans* philicity.

The *trans*-philicity ladders constructed by the six different NMR probes go roughly parallel. Indeed all ladders are almost similar, but some minor deviations related with the position of L in the rungs of the *trans*-philicity ladders are observed.

Linear relationships between the σ^{iso}(SO) X *trans*-philicity descriptors and the R(Pt–X) descriptors of *trans*-influence demonstrate the relation of *trans*-philicity with *trans*-influence phenomenon, thus validating its use as a unified concept in the realm of inorganic, organometallic, coordination chemistry and catalysis. According to the linear relationships for the σ^{iso}(SO) X (X = ^1H, ^{13}CO, $^{17}OH_2$, $^{13}CH_3$, NH_2 and ^{35}Cl) *vs.* R(Pt–X) correlations the increase of the R(Pt–X) descriptor increases the upfield shifts of the σ^{iso}(SO) X shielding constants.

All linear relationships for the σ^{iso}(SO) X (X = ^1H, ^{13}CO, $^{17}OH_2$, $^{13}CH_3$, NH_2 and ^{35}Cl) *vs.* WBI(Pt–X) correlations showed that the increase of WBI(Pt–X) (increase of the covalency of the Pt–X bond) increases the downfield shift of σ^{iso}(SO) X shielding constants. Furthermore the increase of electron density on the Pt central atom increases the upfield shifts of the σ^{iso}(SO) X (X = ^1H, ^{13}CO, $^{17}OH_2$, $^{13}CH_3$, NH_2 and ^{35}Cl) shielding constants.

Conflicts of interest

There are no conflicts to declare.

Notes and references

1 R. G. Wilkins, *The study of kinetics and mechanism of reactions of transition metal complexes*, Allyn and Bacon, Boston, 1974, p. 229.
2 J. E. Huheey, *Inorganic Chemistry*, Harper and Row, New York, 2nd edn, 1978, pp. 498–503.
3 M. L. Tobe, *Inorganic Reaction Mechanisms*, Nelson, Southampton, Great Britain, 1972, vol. 191, pp. 58–88.
4 F. Basolo and R. G. Pearson, *Prog. Inorg. Chem.*, 1962, **4**, 381–453.
5 J. D. Atwood and T. L. Brown, *J. Am. Chem. Soc.*, 1975, **97**, 3380.
6 J. D. Atwood and T. L. Brown, *J. Am. Chem. Soc.*, 1976, **98**, 3155.
7 J. D. Atwood and T. L. Brown, *J. Am. Chem. Soc.*, 1976, **98**, 3160.
8 D. L. Lichtemberger and T. L. Brown, *J. Am. Chem. Soc.*, 1978, **100**, 366.
9 A. Pidcock, R. E. Richards and L. M. Venanzi, *J. Chem. Soc. A*, 1966, 1707–1710.
10 C. A. Tsipis, *Dalton Trans.*, 2019, **48**, 1814–1822.
11 G. Butler, J. Chatt, G. J. Leigh and C. J. Pickett, *J. Chem. Soc., Dalton Trans.*, 1979, 113–116.
12 J. Chatt, C. T. Kan, G. J. Leigh, C. J. Pickett and D. R. Stanley, *J. Chem. Soc., Dalton Trans.*, 1980, 2032–2038.
13 J. Chatt, *Coord. Chem. Rev.*, 1982, **43**, 337–347.
14 C. A. Tsipis, *J. Comput. Chem.*, 2019, **40**, 2550–2562.
15 M. J. Frisch, G. W. Trucks, H. B. Schlegel, G. E. Scuseria, M. A. Robb, J. R. Cheeseman, G. Scalmani, V. Barone, B. Mennucci, G. A. Petersson, H. Nakatsuji, M. Caricato, X. Li, H. P. Hratchian, A. F. Izmaylov, J. Bloino, G. Zheng, J. L. Sonnenberg, M. Hada, M. Ehara, K. Toyota, R. Fukuda, J. Hasegawa, M. Ishida, T. Nakajima, Y. Honda, O. Kitao, H. Nakai, T. Vreven, J. A. Montgomery Jr., J. E. Peralta, F. Ogliaro, M. Bearpark, J. J. Heyd, E. Brothers, K. N. Kudin, V. N. Staroverov, R. Kobayashi, J. Normand, K. Raghavachari, A. Rendell, J. C. Burant, S. S. Iyengar, J. Tomasi, M. Cossi, N. Rega, M. J. Millam, M. Klene, J. E. Knox, J. B. Cross, V. Bakken, C. Adamo, J. Jaramillo, R. Gomperts, R. E. Stratmann, O. Yazyev, A. J. Austin, R. Cammi, C. Pomelli, J. W. Ochterski, R. L. Martin, K. Morokuma, V. G. Zakrzewski, G. A. Voth, P. Salvador, J. J. Dannenberg, S. Dapprich, A. D. Daniels, Ö. Farkas, J. B. Foresman, J. V. Ortiz, J. Cioslowski and D. J. Fox, *Gaussian 09, Revision D.01*, Gaussian, Inc., Wallingford, CT, 2010.
16 J. P. Perdew, K. Burke and M. Ernzerhof, *Phys. Rev. Lett.*, 1996, 77, 3865.
17 J. P. Perdew, M. Ernzerhof and K. Burke, *J. Chem. Phys.*, 1996, **105**, 9982–9985.
18 M. Ernzerhof and G. Scuseria, *J. Chem. Phys.*, 1999, **110**, 5029.

19 C. Adamo and V. Barone, *J. Chem. Phys.*, 1999, **110**, 6158.

20 D. A. Pantazis, X.-Y. Chen, C. R. Landis and F. Neese, *J. Chem. Theory Comput.*, 2008, **4**, 908.

21 EMSL basis set exchange, accessed 08-01-2013, https://bse.pnl.gov/bse/portal.

22 J. Tomasi, B. Mennucci and R. Cammi, *Chem. Rev.*, 2005, **105**, 2999–3093.

23 A. E. Reed, L. A. Curtiss and F. Weinhold, *Chem. Rev.*, 1988, **88**, 899.

24 F. Weinhold, in *The Encyclopedia of Computational Chemistry*, ed. P. V. R. Schleyer, John Wiley & Sons, Chichester, UK, 1998.

25 R. Ditchfield, *Mol. Phys.*, 1974, **27**, 789–807.

26 J. Gauss, *J. Chem. Phys.*, 1993, **99**, 3629–3643.

27 E. van Lenthe, J. G. Snijders and E. J. Baerends, *J. Chem. Phys.*, 1996, **105**, 6505–6516.

28 E. van Lenthe, A. E. Ehlers and E. J. Baerends, *J. Chem. Phys.*, 1999, **110**, 8943–8953.

29 ADF 2012, SCM, Theoretical Chemistry, Vrije Universiteit, Amsterdam, The Netherlands, accessed Feb 15, 2014, http://www.scm.com.

30 (*a*) A. H. Greif, P. Hrobárik, V. Hrobáriková, A. V. Arbuznikov, J. Autschbach and M. Kaupp, *Inorg. Chem.*, 2015, **54**, 7199–7208; (*b*) A. E. Shilov and G. B. Shul'pin, *Chem. Rev.*, 1997, **97**, 2879.

31 J. A. Labinger and J. E. Bercaw, *Nature*, 2002, **417**, 507.

32 A. S. Goldman and K. I. Goldberg, *ACS Symp. Ser.*, 2004, **885**, 1–43.

33 R. Waterman, *Organometallics*, 2013, **32**, 7249–7263.

34 H. Braunschweig, P. Brenner, R. D. Dewhurst, F. Guethlein, J. O. C. Jimenez-Halla, K. Radacki, J. Wolf and L. Zöllner, *Chem. – Eur. J.*, 2012, **18**, 8605–8609.

35 Y.-P. Ho, S. C. F. Au-Yeung and K. K. W. To, *Med. Res. Rev.*, 2003, **23**, 633–655.

36 Y. Jung and S. J. Lippard, *Chem. Rev.*, 2007, **107**, 1387–1407.

37 H.-K. Liu and P. J. Sadler, in *NMR of Biomolecules: Towards Mechanistic Systems Biology*, ed. I. Bertini, K. S. McGreevy and G. Parigi, Wiley-VCH Verlag GmbH & Co. KGaA, 2012, ch. 16, pp. 282–296.

38 T. G. Appleton, C. Clark and L.-E. Manzer, *Coord. Chem. Rev.*, 1973, **10**, 335–422.

39 Z. Chval, M. Sip and J. V. Burda, *J. Comput. Chem.*, 2008, **29**, 2370–2381.

40 J. Chatt and B. L. Shaw, *J. Chem. Soc. Resumed*, 1962, 5075.

41 L. Abis, A. Sen and J. Halpern, *J. Am. Chem. Soc.*, 1978, **100**, 2915–2916.

42 C. M. Jensen and W. C. Trogler, *J. Am. Chem. Soc.*, 1986, **108**, 723–729.

43 D. L. Packett and W. C. Trogler, *Inorg. Chem.*, 1988, **27**, 1768–1775.

44 D. Ramprasad, H. J. Yue and J. A. Marsella, *Inorg. Chem.*, 1988, **27**, 3151–3155.

45 A. H. Greif, P. Hrobárik and M. Kaupp, *Chem. – Eur. J.*, 2017, **23**, 9790–9803.

46 M. P. Mitoraj and A. Michalak, *Inorg. Chem.*, 2010, **49**, 578–582.

47 T. R. Kégl, L. Kollár and T. Kégl, *Adv. Chem.*, 2016, 1–7.